

# Metal-Nitrogen Co-doped Porous Carbon Nanoparticles as Reversible Oxygen Reduction/Evolution Electrodes

**Bitu Bayatsarmadi, Shi Zhang Qiao**

School of Chemical Engineering, the University of Adelaide  
Adelaide, SA 5005, Australia

Bitu.bayatsarmadi@adelaide.edu.au; S.qiao@Adelaide.edu.au

**Abstract** -A series of porous carbon nanoparticles co-doped with nitrogen and non-precious metal including iron and cobalt were prepared by a facile and low-cost soft-templating procedure as reversible oxygen reduction/evolution catalysts. The most active catalyst exhibited an extraordinary activity towards oxygen reduction reaction (ORR) in alkaline medium showing low onset potential (-0.025 V vs Ag/AgCl), high ORR kinetic current (14.5 mA/cm<sup>2</sup>), high selectivity (electron transfer number=4) and excellent electrochemical stability (retained %93 after 60000 seconds). The same hybrid is also highly active for oxygen evolution reaction (OER) in alkaline solution with low onset potential (1.6 V vs RHE) and low Tafel slope (74 mVdec<sup>-1</sup>), making it a high-performance non-precious metal-based catalyst for both ORR and OER. The achieved superior performance as compared to metal-free catalysts and commercial catalysts was attributed to their well-defined porous structures with a narrow mesopore size distribution, large BET surface area, high pore volume, high conductivity and presence of abundant metal-N active sites. This study may pave the way of feasibly designing high efficient catalysts for ORR and OER which are potentially useful for rechargeable metal-air batteries, fuel cells and other important clean energy devices.

**Keywords:** Metal-Nitrogen co-doped carbon nanoparticles, porous structure, soft-template, reversible electrode, oxygen reduction/evolution reaction.

## 1. Introduction

Energy is a central challenge in today's society due to population growth, energy consumption increment and finite reserves for fossil fuels. Based on rapid depletion of fossil fuels as well as significant increase in greenhouse gas emissions and global climate changes, alternative energy storage and conversion systems such as fuel cells, metal-air batteries and water splitting devices have attracted researchers' attention (Fillol et al. 2011; Manthiram et al. 2008; Subbaraman et al. 2012). All aforementioned sustainable energy sources closely associated with a core process, oxygen reduction/evolution reaction (ORR/OER) that is initiated at the boundary of multiple phases (solid, liquid and gas) (Yuan et al. 2014; Zhang, de Respinis & Frei 2014). However, the sluggish kinetics of ORR/OER in nature significantly decreases the energy conversion efficiency, which therefore underlines the importance of designing an optimal electrode structure involving high performance catalysts to reduce the reaction barrier and facilitate the reaction kinetics (Kinoshita 1988). To develop low-cost alternative catalysts with high activity and durability in ORR/OER, great efforts have been devoted to synthesizing carbon-based materials due to their low-cost, high stability, excellent activity and high durability against fuel methanol and CO, especially in alkaline medium (Li & Antonietti 2013). Among the carbon-based materials, carbon nanoparticles with ordered meso-structures and controlled morphologies have great advantages because of their remarkable properties including high surface area and the diffusion channels for fast mass transfer (Liang, J et al. 2013). The mesopores with high specific surface areas and large pore volumes not only allow facile access of reactants to the active sites of catalysts and favour mass transport of the intermediate species, but also lead to enhanced electron delivery to the active centres due to the continuous framework structure (Oh et al. 2012).

Synthesizing heteroatom-doped carbon materials due to their unique electronic properties and structural features have been recently evolved into metal-free catalysts, although their ORR/OER performance is still far inferior to the commercial catalysts. Co-doping of nitrogen doped carbon catalysts with non-precious metals such as cobalt and iron can improve ORR/OER catalytic activity nitrogen-doped carbon materials. Elemental composition, interaction between different components, specific surface area and porous structure of the non-precious metal and nitrogen co-doped carbon materials are the crucial factors which govern the performance of this type of catalysts (Liang, H-W et al. 2013). Although some breakthrough works have been recently reported by selection of non-precious metal and nitrogen precursors and carbon supports, developing new materials with high activity, durability and strong long-term stability compared to commercialized catalysts still remains a challenge.

To address these issues, here we prepared a series of porous carbon nanoparticles co-doped with nitrogen and non-precious metal including iron (denoted as Fe-N-PC) and cobalt (denoted as Co-N-PC) by a facile and low-cost soft-templating procedure as reversible oxygen evolution catalysts. These catalysts have been successfully synthesized using F127 and CTAB as soft-templates, Aminophenol-formaldehyde resin as both carbon and nitrogen precursor, iron (III) chloride hexahydrate and cobalt (II) chloride hexahydrate as iron and cobalt precursors, respectively. The synthesized materials have been applied as electrocatalysts in reversible oxygen reduction reaction. The well-structured mesoporosity and abundant surface defect sites assure an efficient ORR/OER catalytic performance of these materials, showing a high activity, better durability and methanol tolerance ability as compared to the commercial catalysts.

## 2. Material and Methods

### 2. 1. Chemicals

Pluronic (F127), Hexadecyltrimethylammonium bromide (CTAB,  $\geq 98\%$ ), 3-Aminophenol ( $C_6H_7NO$ , 98%), Iron (III) chloride hexahydrate ( $FeCl_3 \cdot 6H_2O$ ) and Cobalt (II) chloride hexahydrate ( $CoCl_2 \cdot 6H_2O$ ) were purchased from Sigma-Aldrich. Formaldehyde solution (HCHO, 37/10) and ethanol (EtOH, absolute) were purchased from Chem-Supply. Highly purified water (DI water,  $>18 M\Omega$  cm resistivity) was provided by a PALL PURELAB Plus system. All chemicals were directly used without any further treatment and purification.

### 2. 2. Material Synthesis

In a typical synthesis, 0.5 g of fully dissolved F127 in 40 ml of EtOH was added to 100 ml of DI-water at 25°C. Then 0.65 g CTAB was added to the solution and kept stirred for 30 minutes. Next, 1.0 g 3-Aminophenol was added and stirred until a complete dissolution followed by introduction of 1.4 mL (37 wt. %) formaldehyde and stirred for another 30 minutes. Afterwards, a given amount of  $FeCl_3 \cdot 6H_2O$  or  $CoCl_2 \cdot 6H_2O$  (1 wt. %) was added to the mixture and kept stirring at 25°C for 24 hours. Finally, the mixture was transferred to a Teflon-lined autoclave for hydrothermal reaction at 100 °C for 24 h. The resulting solid polymers were collected by vacuum filtration followed by washing with DI-water and ethanol for 3 times and drying at 100°C for 24 hours. This washing step leads to remove the free metal species which were accessible outside of carbon framework. Fe-N-PC or Co-N-PC nanoparticles were obtained by calcination of solid polymers under  $N_2$  flow in the tubular furnace at 350°C using heating rate of (1°C/min) for 3 hours to remove the template followed by carbonization at 900°C with heating rate of (2°C/min) for 4 hours under  $N_2$  flow. For comparison purposes, metal-free catalysts (N-PC) were synthesized using the same synthesizing procedure.

### 2. 3. Material Characterization

The morphology of synthesized samples was characterized by transmission electron microscope (FEI Tecnai G2 Spirit TEM) operating at 120 kV and scanning electron microscope (FEI Quanta 450 ESEM) operating at 10 kV. Nitrogen adsorption-desorption isotherms were measured on Tristar II (Micrometrics) at -196 °C. Pore size distributions were calculated by Barrett-Joyner-Halenda (BJH) model using the data

of adsorption branch on the isotherm. The specific surface areas were calculated using adsorption data at the relative pressure range of  $P/P_0 = 0.05-0.3$  by Brunauer-Emmett-Teller (BET) model. The total pore volumes were estimated from the adsorbed amounts at a relative pressure ( $P/P_0$ ) of 0.994. All the samples were degassed at 150°C for more than 6 h prior to the Nitrogen sorption tests. Raman spectra were collected on LabRAM (Horiba Ltd) with 532 nm laser. X-ray diffraction (XRD) patterns were collected on a powder X-ray diffractometer at 40 kV and 15 mA using Co-K $\alpha$  radiation (Miniflx-600, Rigaku).

## 2. 4. Electrode Preparation and Electrochemical Measurements

All the electrochemical measurements were performed under identical conditions (the same catalyst mass loading). In a typical electrode preparation, 2.0 mg of synthesized catalyst was ultrasonically dispersed in 0.5 ml 0.5 % Nafion aqueous solutions. 20  $\mu$ L of catalyst dispersion (4.0 mg mL<sup>-1</sup>) was then transferred onto the glassy carbon rotating disk electrode (RDE, 0.196 cm<sup>2</sup>, Pine Research Instrumentation, USA) via a controlled drop casting approach and dried in ambient environment for 1 h and served as a working electrode. 0.1 M KOH aqueous solution was used as the electrolyte which was purged with O<sub>2</sub>/N<sub>2</sub> for at least 30 min to achieve O<sub>2</sub>/N<sub>2</sub>-saturated solution for ORR/OER tests, respectively. The reference electrode was an Ag/AgCl in 4M KCl solution and the counter electrode was platinum wire. The current density was normalized to the geometric surface area and the measured potentials vs. Ag/AgCl were converted to a reversible hydrogen electrode (RHE) scale according to the Nernst equation;

$$E_{RHE} = E_{Ag/AgCl} + 0.059 \times pH + 0.205 \quad (1)$$

The OER/ORR polarization curves were recorded with the scan rate of 0.5 mV<sup>-1</sup>. The working electrodes were scanned for several times until the signals were stabilized, and then the data for polarization curves were collected, corrected for iR contribution within the cell. The Tafel slope was calculated according to the following equation:

$$\eta = b \cdot \log(j/j_0) \quad (2)$$

Where  $\eta$  denotes the overpotential,  $b$  denotes the Tafel slope,  $j$  denotes the current density and  $j_0$  denotes the exchange current density. The onset potentials were determined based on the beginning of the linear region in Tafel slope. The overpotential was calculated as follows:

$$\eta = E(\text{vs. RHE}) - 1.23 \quad (3)$$

Considering O<sub>2</sub>/H<sub>2</sub>O equilibrium at 1.23 V vs. RHE.

The overall electron transfer numbers per oxygen molecule involved in a typical ORR process can be calculated from the slopes of Koutecky-Levich plots using the following equation:

$$1/j_D = 1/j_K + 1/(B\omega^{1/2}) \quad (4)$$

Where  $j_K$  is the kinetic current density in mAcm<sup>-2</sup> at a constant potential,  $j_D$  is the measured current density on RDE,  $\omega$  is the electrode rotating speed in rpm, and  $B$  is the reciprocal of the slope, which could be determined from the slope of Koutecky-Levich plot using Levich equation:

$$B = 0.2nF(v) - 1/6C_{O_2}(D_{O_2})^{2/3} \quad (5)$$

Where  $n$  is the number of electrons transferred per oxygen molecule,  $F$  is the Faraday constant,  $v$  is the kinetic viscosity,  $C_{O_2}$  is the bulk concentration of O<sub>2</sub>, and  $D_{O_2}$  is the diffusion coefficient of O<sub>2</sub> in 0.1 M KOH. The constant 0.2 is adopted when the rotating speed is expressed in rpm.

The stability tests were performed at a static potential of  $-0.3\text{V}$  vs.  $\text{Ag}/\text{AgCl}$  at room temperature in the  $\text{O}_2$ -saturated  $0.1\text{M}$   $\text{KOH}$  aqueous electrolyte. The methanol tolerance of materials was tested under the same condition before and after adding methanol to electrolyte.

### 3. Results and Discussions

The metal and nitrogen co-doped porous carbon nanoparticles (M-N-PC) were synthesized via a dual soft-templating technique. The first synthesis step involved in the formation of micelles by the combination of two surfactants (F127 and CTAB) followed by polymerization of aminophenol and formaldehyde precursors on the surface of micelles to form a resol-micelle complex through a sol-gel process at  $30^\circ\text{C}$ . Next, metal precursors such as cobalt (II) chloride hexahydrate and iron (III) chloride hexahydrate were introduced to the system. Following the cross-linking of metal-contained resol and the aggregation of nanomicelles under a hydrothermal treatment at  $100^\circ\text{C}$ , the as-synthesized porous polymer nanoparticles were obtained. In second step, the dried solid products were subjected to heating at  $350^\circ\text{C}$  (rate of  $1.5^\circ\text{C}/\text{min}$ ) for 3 h under  $\text{N}_2$  flow to remove the soft templates. During the template removal, plenty of pores were formed due to the volatilization of small organic moieties and rearrangement of carbon atoms. Finally metal and nitrogen doped porous carbon nanoparticles were produced by direct carbonization at  $900^\circ\text{C}$  (rate of  $2^\circ\text{C}/\text{min}$ ) for 4 h under  $\text{N}_2$  flow.

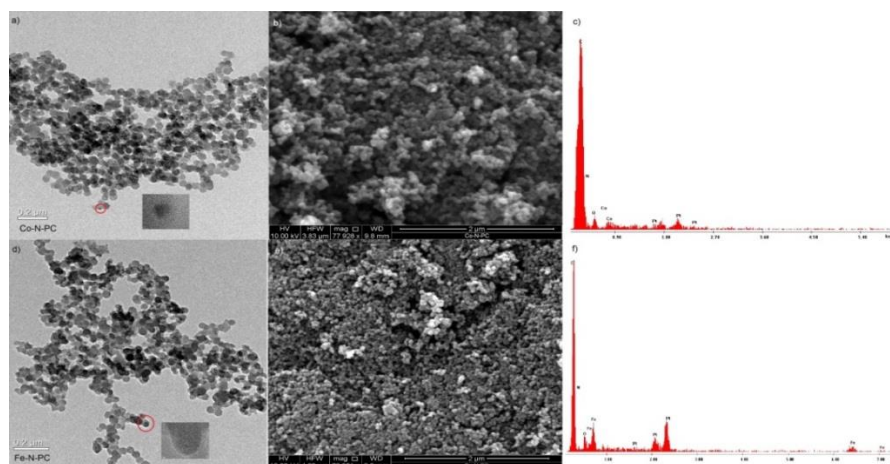


Fig. 1. SEM images (a,d), TEM images (b,e) and EDS spectra of synthesized M-N-PC nanoparticles (c,f)

The morphology of M-N-PC nanoparticles was first investigated by scanning electron microscopy (SEM) and transmission electron microscopy (TEM). The SEM images show that both Co-N-PC and Fe-N-PC nanoparticles are approximately spherical in morphology and they are in the same dimensions (Fig. 1a,d). TEM images confirm the spherical morphology with average particle diameter of  $100\text{ nm}$  (Fig. 1b,e). Both SEM and TEM images show that spheres are randomly stacked together which might be attributed to defective structure of synthesized spheres due to presence of doped nitrogen and metal species (Sheng et al. 2011). The energy-dispersive spectra (EDS) of both samples exhibit the presence of related metal species, nitrogen dopant, oxygen and carbon in the structure of synthesized materials (Fig. 1c,f).

The surface area and porosity of synthesized samples were characterized using nitrogen adsorption-desorption technique. The isotherms of the Fe-N-PC and Co-N-PC (Fig. 2a) exhibit the same type IV curve with a distinct capillary condensation step at relative pressure ( $P/P_0$ ) of  $0.4-0.7$  and a  $\text{H}_1$  hysteresis loop, indicative of uniform ordered pores. The sharp step at  $P/P_0=0.9-1$  corresponds to the capillary condensation of nitrogen inside the extra-large mesopores/macropores which were created by stacking the spheres together. This may be due to the fact that synthesized samples have structural defects caused by the incorporation of nitrogen and metal species into the carbon framework. The rapid rise in the low pressure region ( $P/P_0<0.05$ ) for both samples suggests the existence of micropores in the synthesized

nanoparticles (Yu et al. 2014). The pore size distributions (Fig.2b) show sharp peaks at 3.6 nm and 3.7 nm for Fe-N-PC and Co-N-PC, respectively which confirms the uniform pore structures of synthesized nanoparticles. The BET surface area of Fe-N-PC and Co-N-PC are 443.83 and 483.99  $\text{m}^2\text{g}^{-1}$  and total pore volumes are calculated as 0.49 and 0.53  $\text{m}^3\text{g}^{-1}$ , respectively.

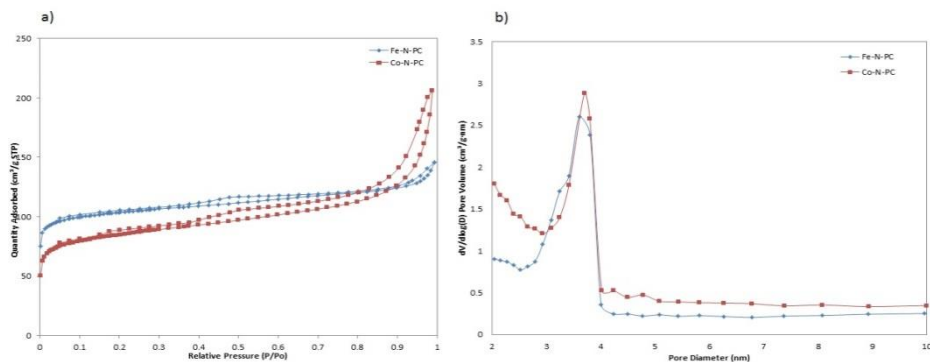


Fig. 2. (a) Nitrogen adsorption-desorption isotherm and (b) pore size distribution of M-N-PC nanoparticles

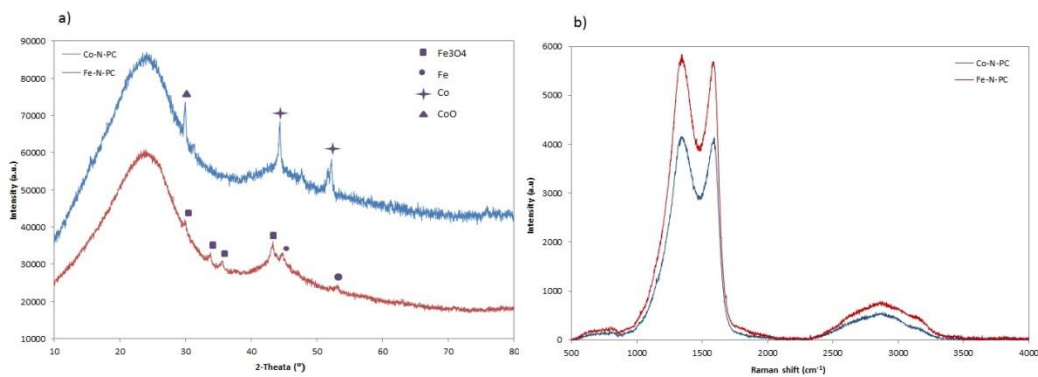


Fig. 3. (a) Wide-angle XRD patterns, (b) Raman spectra of synthesized M-N-PC nanoparticles.

Wide-angle XRD patterns (Fig.3a) show diffraction peaks at  $2\theta=23-24^\circ$  which are usually attributed to the (002) plane of the graphitic carbon. For Co-N-PC nanoparticles, the peak at  $28^\circ$  can be ascribed to CoO and peaks at  $44^\circ$  and  $52^\circ$  can be assigned to metallic Co (Jin et al. 2015). Furthermore, peaks at  $29^\circ$ ,  $32^\circ$ ,  $36^\circ$  are associated with  $\text{Fe}_3\text{O}_4$  and peaks at  $43^\circ$ ,  $45^\circ$  and  $53^\circ$  are ascribed to metallic Fe (Liang et al. 2014).

Raman spectra of both samples were also collected to further assess the graphitic structure of materials. As shown in Fig. 3b, Typical G bands representing the  $\text{sp}^2$ -hybridized graphitic carbon atoms ( $\sim 1580 \text{ cm}^{-1}$ ) and D bands resulting from the disordered carbon frames on the defect sites ( $\sim 1350 \text{ cm}^{-1}$ ) were obtained. The  $I_G/I_D$  ratio in Co-N-PC nanoparticles and Fe-N-PC nanoparticles are calculated as 0.99 and 0.97, respectively indicating slightly higher-graphitic structure was formed in Co-N-PC sample.

To evaluate the ORR catalytic performance of the synthesized nanoparticles, cyclic voltammetry (CV) was firstly conducted. As shown in Fig. 4a, Co-N-PC nanoparticles showed a distinct ORR peak centered at 0.75 V (vs. RHE) which is about 140 mV and 194 mV more positive than Fe-N-PC and N-PC, respectively. Linear sweep voltammetry (LSVs) have been monitored using a rotating disk electrode (RDE) in  $\text{O}_2$ -saturated electrolyte to further investigate the ORR activity. The onset potential and reaction current density of synthesized materials were acquired from LSVs at 1600 rpm (Fig. 4b). Remarkably, Co-N-PC showed lowest onset potential and highest reaction current density at certain overpotential, suggesting the presence of highest number of active site and fastest reaction kinetics of Co-N-PC nanoparticles among other samples. A series of LSVs were also recorded from 400 to 2400 rpm for Co-N-

PC nanoparticles (Fig. 4c) which show reaction current growth by increasing the rotation speed. Inset of Fig. 4c presents the Koutecky-Levich plots of Fe-N-PC nanoparticles at different potential obtained from RDE at several rotation rates. Accurate electron transfer numbers ( $n$ ) and kinetic current density ( $J_k$ ) were calculated through K-L plots (Fig. 4d) and suggesting that oxygen can be reduced on Co-N-PC catalysts in four electron ( $4e^-$ ) reaction pathway with high limiting current density ( $14.5 \text{ mA/cm}^2 @ -0.5 \text{ V vs. Ag/AgCl}$ ).

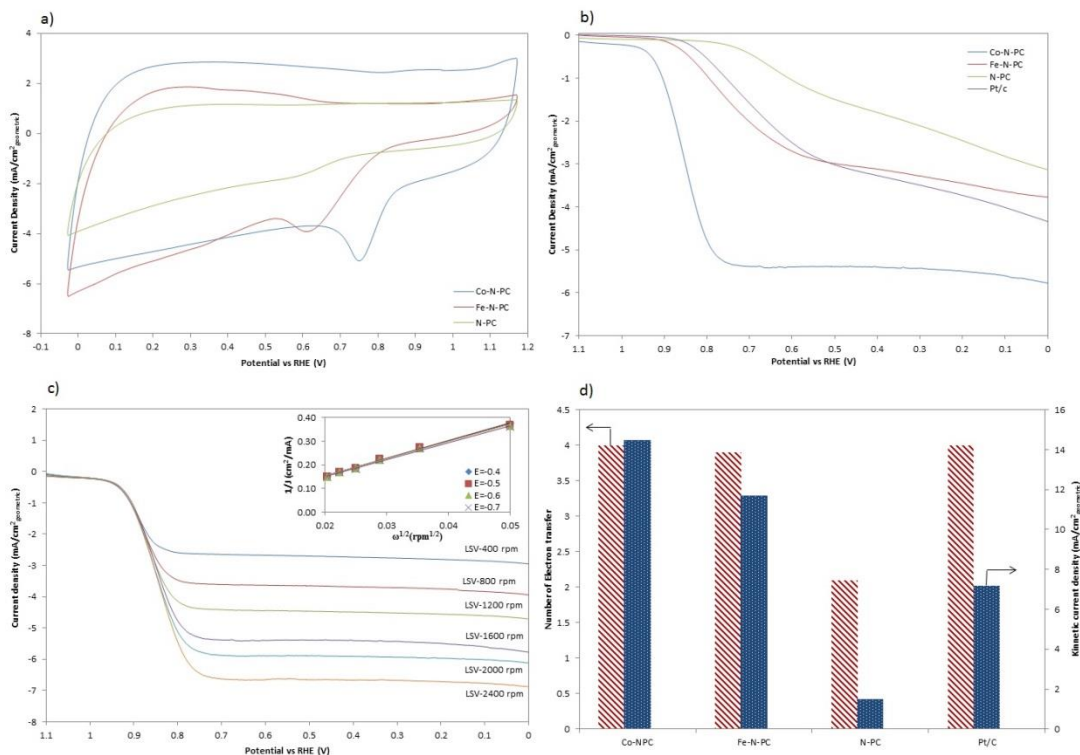


Fig. 4. (a) CVs of ORR on the synthesized electrocatalysts in an  $\text{O}_2$ -saturated 0.1 M KOH solution (scan rate:  $100 \text{ mV s}^{-1}$ ). (b) LSVs of synthesized electrocatalysts on a RDE (1600 rpm, scan rate:  $5 \text{ mV s}^{-1}$ ), (c) LSVs and (inset of c) K-L plots of Co-N-PC nanoparticles on a RDE at different rotating speeds from 400 rpm to 2400 rpm, (d) summary of the kinetic current ( $J_k$ ) and the electron transfer number ( $n$ ) on the basis of RDE data at  $-0.5 \text{ V vs Ag/AgCl}$ .

The OER activity of synthesized materials was examined by LSV (Fig. 5a). The Co-N-PC nanoparticles exhibits a sharp onset potential at 1.6 V vs. RHE with enhanced OER current, indicating the Co-N active sites significantly improved the catalytic activity compared to Fe-N-PC nanoparticles and metal-free sample. Furthermore, this catalyst affords a current density of  $10 \text{ mA/cm}^2$  at 1.8 V which is lower than other synthesized materials. Also, the Tafel slope value (Fig. 5b) of Co-N-PC ( $74 \text{ mVdec}^{-1}$ ) is lower than that of Fe-N-PC ( $192 \text{ mVdec}^{-1}$ ), N-PC ( $318 \text{ mVdec}^{-1}$ ) and  $\text{IrO}_2/\text{N-PC}$  ( $144 \text{ mVdec}^{-1}$ ), suggesting its favourable OER kinetics.

The durability of selected electrocatalyst (Co-N-PC nanoparticles) was evaluated by the chronoamperometric response under a constant voltage of  $-0.3 \text{ V}$  (Fig. 6a) which exhibits a reliable stability, retaining 93% of the initial current after 60000 seconds. The methanol tolerance ability of selected catalyst was tested by monitoring the ORR current after the addition of methanol into the electrolyte solution (with the resulting methanol concentration of 3M). As shown in Fig. 6b, there is no significant change under  $-0.3 \text{ V}$  after the addition of methanol into the electrolyte, suggesting the high selectivity of Co-N-PC catalyst towards reversible oxygen evolution electrode to avoid crossover effects.

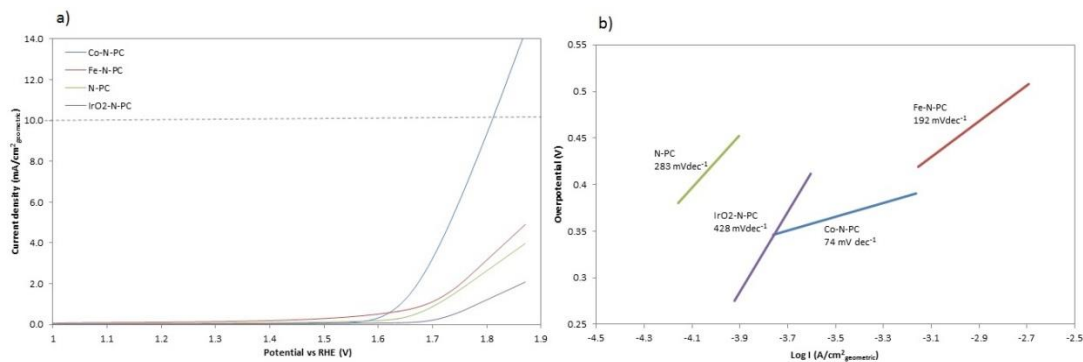


Fig. 5. (a) LSVs of synthesized electrocatalysts on a RDE (1600 rpm, scan rate: 5 mV s<sup>-1</sup>), (b) Tafel plots of synthesized electrocatalysts in an O<sub>2</sub>-saturated 0.1 M KOH solution (scan rate of 5 mV s<sup>-1</sup>).

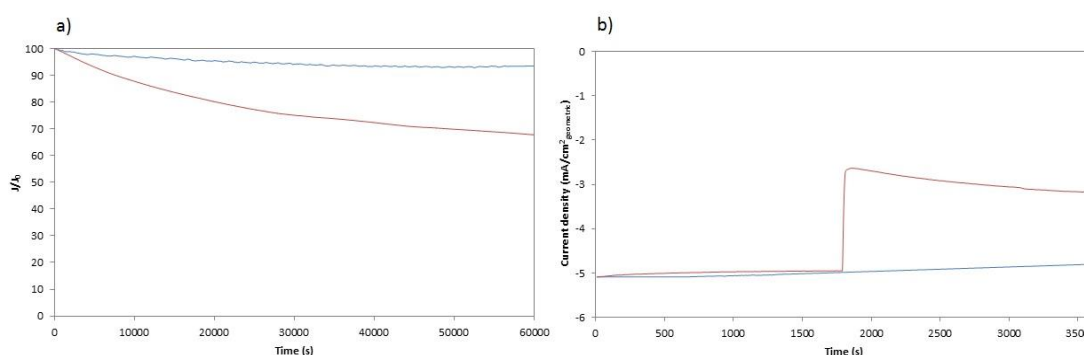


Fig. 6. The chronoamperometric response of Co-N-PC nanoparticles and commercial Pt/C at -0.3 V (a) after 60000 s, (b) after methanol addition

#### 4. Conclusion

In summary, metal and nitrogen co-doped porous carbon nanoparticels has been synthesized via simple and low-cost soft-templating method with good conductivity, meso/micro pore structure, high pore volume and large surface area to catalyze the reversible electron reduction of oxygen. The synthesized electro-catalyst exhibit higher ORR/OER activity, more favorable kinetics, stronger stability and durability than those of Fe-N-PC, metal-free NPC and commercial catalysts. The excellent catalytic performance of Co-N-PC nanoparticles can be attributed to the porous structure, large active surface area, strong structural stability and improved mass/charge transport. This novel approach for fabrication of Co-N-PC nanoparticles could have flexibility in tailoring the composition, mesoporosity, morphology and graphitic structure which may open a space for the preparation of other metal and nitrogen co-doped carbon materials with even higher performance.

#### Acknowledgements

This research is financially supported by Australian Research Council (DP1095861, DP130104459).

#### References

- Fillol, J.L., Codolà, Z., Garcia-Bosch, I., Gómez, L., Pla, J.J., & Costas, M. (2011). Efficient Water Oxidation Catalysts Based On Readily Available Iron Coordination Complexes. *Nat Chem*, 3(10), 807-813.
- Jin, H., Wang, J., Su, D., Wei, Z., Pang, Z., & Wang, Y. (2015). In-Situ Cobalt-Cobalt Oxide/N-Doped Carbon Hybrids As Superior Bi-Functional Electrocatalysts For Hydrogen And Oxygen Evolution. *Journal of the American Chemical Society*.
- Kinoshita, K. (1988). *Carbon: Electrochemical and Physicochemical Properties*. Wiley-Interscience.

- Li, X-H., & Antonietti, M. (2013). Polycondensation of Boron- and Nitrogen-Codoped Holey Graphene Monoliths from Molecules: Carbocatalysts for Selective Oxidation. *Angewandte Chemie International Edition*, 52(17), 4572-4576.
- Liang, H-W., Wei, W., Wu, Z-S., Feng, X., & Müllen, K. (2013). Mesoporous Metal–Nitrogen-Doped Carbon Electrocatalysts for Highly Efficient Oxygen Reduction Reaction. *Journal of the American Chemical Society*, 135(43), 16002-16005.
- Liang, J., Du, X., Gibson, C., Du, XW., & Qiao, S.Z. (2013). N-Doped Graphene Natively Grown on Hierarchical Ordered Porous Carbon for Enhanced Oxygen Reduction. *Advanced Materials*, 25(43), 6226-6231.
- Liang, J., Zhou, R.F., Chen, X.M., Tang, Y.H., & Qiao, S.Z. (2014). Fe–N Decorated Hybrids of CNTs Grown on Hierarchically Porous Carbon for High-Performance Oxygen Reduction. *Advanced Materials*, 26(35), 6074-6079.
- Manthiram, A., Vadivel, A., Sarkar, A., & Muraliganth, T. (2008). Nanostructured Electrode Materials For Electrochemical Energy Storage And Conversion. *Energy & Environmental Science*, 1(6), 621-638.
- Oh, S.H., Black, R., Pomerantseva, E., Lee, J-H., & Nazar, L.F. (2012). Synthesis Of A Metallic Mesoporous Pyrochlore As A Catalyst For Lithium–O<sub>2</sub> Batteries. *Nat Chem*, 4(12), 1004-1010.
- Sheng, Z-H, Shao, L, Chen, J-J, Bao, W-J, Wang, F-B, & Xia, X-H. (2011). Catalyst-Free Synthesis of Nitrogen-Doped Graphene via Thermal Annealing Graphite Oxide with Melamine and Its Excellent Electrocatalysis. *ACS Nano*, 5(6), 4350-4358.
- Subbaraman, R, Tripkovic, D, Chang, K-C, Strmcnik, D, Paulikas, AP, Hirunsit, P, Chan, M, Greeley, J, Stamenkovic, V., & Markovic, NM. (2012). Trends In Activity For The Water Electrolyser Reactions On 3d M(Ni,Co,Fe,Mn) Hydr(Oxy)Oxide Catalysts. *Nat Mater*, 11(6), 550-557.
- Yu, J., Guo, M., Muhammad, F., Wang, A., Yu, G., Ma, H., & Zhu, G. (2014). Simple Fabrication Of An Ordered Nitrogen-Doped Mesoporous Carbon With Resorcinol–Melamine–Formaldehyde Resin. *Microporous and Mesoporous Materials*, 190, 117-127.
- Yuan, C, Wu, HB, Xie, Y., & Lou, XW. (2014). Mixed Transition-Metal Oxides: Design, Synthesis, and Energy-Related Applications, *Angewandte Chemie International Edition*, 53(6), 1488-1504.
- Zhang, M, de Respinis, M., & Frei, H. (2014). Time-Resolved Observations Of Water Oxidation Intermediates On A Cobalt Oxide Nanoparticle Catalyst. *Nat Chem*, 6(4), 362-367.